Modelling of Deep-Sea Gravity Currents Using an Integrated Plume Model

Guttorm Alendal, Helge Drange and Peter M. Haugan

Nansen Environmental and Remote Sensing Center, Bergen, Norway

Abstract

An integrated plume model is used to describe large scale gravity currents in the ocean. The model describes competing effects of (negative) buoyancy, friction, entrainment and Coriolis force, as well as a pressure term due to variable plume thickness, on the flux, speed and flow direction of the plume. Equations for conservation of salt and internal energy (temperature) and a full equation of state for seawater is included in the model.

The entrainment of ambient water is parameterized with support in empirical data, and a drag coefficient consistent with the entrainment is introduced.

The model is tested against the overflow through the Denmark Strait, the flow down the Weddell Sea continental slope, and the outflow of saline water through the Gibraltar Strait and from the Spencer Gulf, Australia. The former gain an extra driving mechanism due to the thermobaric effect, while in the two latter cases the initial density difference is so large that this effect is not essential.

Order of magnitude fit with measurements requires drag·coefficient between 0.01 and 0.1. Conditions susceptible to meander behaviour and a singularity arising from the pressure dependency on the current thickness variations are briefly discussed.

Introduction

Buoyancy is the driving force for atmospheric and oceanic phenomena such as snow avalanches, volcanic eruption columns, chimneys, deep water formation, deep sea gravity currents, turbidity currents and thermal vents [Rudnicki and Elderfield, 1992; Simpson, 1987; Turner, 1973; Woods, 1988]. Since the pioneering work of Morton and co-workers [Morton *et al.*, 1956], it has been shown that a set of simple conservation equations can be used to describe the main dynamics of the above mentioned features. This paper elaborates on the dynamics of deep-sea gravity currents, and a dynamic model is derived that represents a slight extension to the gravity current models set up by Smith [1975] and Killworth [1977]. The model also represents an extension of the model used by Speer and Tziperman [1990] since we are treating the salinity and temperature explicitly and we use Richardson number dependent entrainment parameterization. Understanding the dynamics of such currents is also important in view of shallow injection of CO_2 enriched water in the ocean [Haugan and Drange, 1992; Drange *et al.*, 1993].

The Polar Oceans and Their Role in Shaping the Global Environment
Geophysical Monograph 85

The model is developed by integrating the local momentum and continuity equations over a cross-section of the current. This means that interior structures are averaged out and we are describing the currents overall, or bulk, behaviour. The model is steady state excluding time varying phenomena such as upwelling and tidal currents and the influence such events might have. First we give a description of the model introducing a drag coefficient consistent with the Richardson number dependent entrainment parameter. A thorough derivation of the model is given in the appendix. The occurrence of a singularity in the model originating from the inclusion of effects from variation in current thickness is briefly discussed.

We have used measurements from four different sites to test the model: the overflow through the Denmark Strait between Iceland and Greenland, the flow down the Weddell Sea continental slope, the outflow from the Mediterranean through the Gibraltar Strait and the outflow from Spencer Gulf, Australia. The two former are important sites for formation of deep-sea bottom water [Killworth, 1983], and the density difference is mainly caused by the current water being colder than the environment. This gives rise to the thermobaric effect, i.e., cold water has higher compressibility than warmer water. For the two latter currents the excess density is set up by higher salinity in the current relative to the environment.

The model runs are performed as a sensitivity study of the

drag coefficient, since this is the most sensitive parameter. The testing is rough in the sense that we are not performing detailed comparisons of the solutions against measurements. The events are time dependent and the measurements sparse in time and space. Therefore only order of magnitude comparisons with our simple steady state model is justified.

The Integrated Plume Model

The Physical Configuration

The current is assumed to move down an inclined bottom and we distinguish between three different coordinate systems as shown in Fig. 1. The (x, y, z) system has z in the vertical direction and the x- and y-directions in the horizontal plane, while the (x', y', z') system has z' perpendicular to the plane and with x' and y' directions lying in the inclined plane. The x- and x'-directions are similar giving that y- and y'- directions forms an angle θ with each other. We then have the following relations between the marked and the unmarked co-ordinate systems:

$$\mathbf{i}' = \mathbf{i},\ \mathbf{j}' = \cos\theta\,\mathbf{j} - \sin\theta\,\mathbf{k},\ \mathbf{k}' = \sin\theta\,\mathbf{j} + \cos\theta\,\mathbf{k}, \quad (1)$$

where $\mathbf{i}$, $\mathbf{j}$ and $\mathbf{k}$ are the unit vectors in x-, y-, and z-directions, respectively, and $\mathbf{i}'$, $\mathbf{j}'$ and $\mathbf{k}'$ are the corresponding unit vectors in the (x', y', z') system.

The model is developed in the curvi-linear coordinate system (ξ, η, z') which has ξ in the along-stream direction and η perpendicular to both the ξ and the z' direction. The η direction is to the left of the current looking downstream. β is the angle between the along-stream direction and the x-direction and this relates the two coordinate systems fixed to the slope as follows:

$$\mathbf{e}_\xi = \cos\beta\,\mathbf{i} + \sin\beta\,\mathbf{j}', \qquad \mathbf{e}_\eta = -\sin\beta\,\mathbf{i} + \cos\beta\,\mathbf{j}', \quad (2)$$

where $\mathbf{e}_\xi$ is the unit vector in along-stream direction and $\mathbf{e}_\eta$ the unit vector in η direction. Together with $\mathbf{k}'$ these vectors form an orthogonal span of the 3D space. From equations (1) and (2) it follows that

$$\mathbf{k} = \cos\theta\,\mathbf{k}' - \sin\theta\sin\beta\,\mathbf{e}_\xi - \sin\theta\cos\beta\,\mathbf{e}_\eta. \quad (3)$$

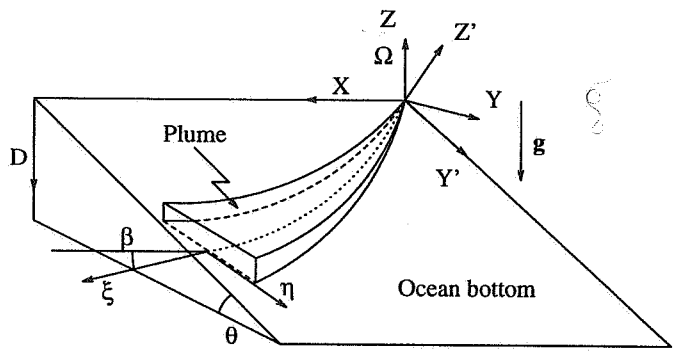

Fig. 1. The physical configuration. Defining the coordinate systems.

and since the (ξ, η, z') system is accelerated relative to the bottom fixed coordinate systems, the fictive centrifugal force

$$\frac{\partial}{\partial\xi}\mathbf{e}_\xi = \frac{\partial}{\partial\xi}\left(\cos\beta\mathbf{i} + \sin\beta\mathbf{j}'\right) = \left(\frac{\partial}{\partial\xi}\beta\right)\mathbf{e}_\eta \quad (4)$$

arises.

Averaging over a cross-section of the current with area $A = w{\cdot}h$, where w (m) and h (m) are, respectively, the width and the height of the current, gives the model equations (subscript ξ means $\partial/\partial\xi$)

$$(\rho A U)_\xi = \rho_e E(Ri)\, w\, U, \quad (5)$$

$$(T\rho A U)_\xi = \rho_e T_e\, E(Ri) w U, \quad (6)$$

$$(S\rho A U)_\xi = \rho_e S_e\, E(Ri) w\, U, \quad (7)$$

$$\left(\rho A U^2\right)_\xi = A g(\rho - \rho_e)(\sin\beta\sin\theta - h_\xi) - C_D\,\rho\, w\, U^2, \quad (8)$$

$$\rho U^2 \beta_\xi = g(\rho - \rho_e)\sin\theta\cos\beta - fU. \quad (9)$$

Here ρ (kg m^{-3}), S (psu) and T (K) is the density, salinity and temperature of the current, respectively, while the corresponding variables with subscript e are connected to the ambient water. U (m s^{-1}) denotes the current mean velocity, E (dimensionless) the entrainment parameter and C_D (dimensionless) the friction parameter, or the drag coefficient.

The Coriolis parameter is given by $f = 2\Omega(\sin\varphi\cos\theta - \cos\varphi\sin\theta\sin\zeta)$ (s^{-1}), φ (rad) being the latitude and ζ (rad) being the orientation of the slope. For $\zeta = 0$ the slope sinks in the eastward direction, while $\zeta = \pi/2$ means that the slope is in the north direction [Alendal *et al.*, 1993].

Equations (5)-(7) are conservation equations for mass, internal energy (heat) and salt, respectively, while the two latter are momentum equations in the along stream direction (8) and in the cross-stream-direction (9). A rigorous derivation of these equations is given in the appendix.

The x and y positions together with the total depth enter the differential system through the geometric relations

$$\frac{\partial}{\partial\xi}x = \cos\beta, \quad \frac{\partial}{\partial\xi}y = \sin\beta\cos\theta, \quad \frac{\partial}{\partial\xi}D = \sin\beta\sin\theta. \quad (10)$$

The equation of state of seawater [UNESCO, 1981] relates the density of seawater to the salinity, temperature and pressure (depth);

$$\rho = \rho(S, T, p). \quad (11)$$

This system of ordinary differential equations is not closed and thereby not solvable until we have an extra relation between some of the variables in the model. We have assumed constant width over thickness ratio

$$\frac{w}{h} = constant. \quad (12)$$

In our numerical study this parameter is set by the initial values of volume flux $F_0 = w_0\, h_0\, U_0$, (m^3 s^{-1}), velocity U_0 and height h_0 (m) of the current.

The Entrainment Parameterization and The Friction Parameter

The entrainment parameter $E(Ri)$ is strongly related to the overall Richardson number for a wall bounded current [Turner, 1973]

$$Ri = \frac{gh(\rho - \rho_e)\cos\theta}{\rho U^2} = \frac{g'h\cos\theta}{U^2}, \qquad (13)$$

where $g' = g\,h\,(\rho - \rho_e)/\rho$, is the reduced gravity. With support in laboratory experiments, Christodoulou [1986] found general laws for this dependency:

$$E(Ri) = \begin{cases} 0.07 & \text{for } Ri < 10^{-2} \\ 0.007 Ri^{-1/2} & \text{for } 10^{-2} < Ri < 1 \\ 0.007 Ri^{-3/2} & \text{for } 1 < Ri < 10^2 \end{cases}, \qquad (14)$$

and

$$E(Ri) = 0.002\,Ri \quad \text{for} \quad 0.08163 < Ri < 12.25. \qquad (15)$$

Throughout this paper equation (14) has been used for the entrainment parameter, with the mean value of (14) and (15) for $0.08163 < Ri < 12.25$.

The friction parameter is usually defined by

$$u_*^2 = C_D u^2, \qquad (16)$$

where u_* ($\mathrm{m\,s^{-1}}$) is the friction velocity. Adopting the Kato-Phillips like equation [Stigebrandt, 1987]

$$E\,u = \left(2\,m_0\,u_*^3\right) / \left(g'\,h\,cos\theta\right), \qquad (17)$$

where m_0 is a constant of order 1 [Stigebrandt, 1987; Oberhuber, 1993] and solving (16) and (17) with respect to C_D gives

$$C_D^{3/2} = \frac{Ri\,E(Ri)}{2\,m_0}. \qquad (18)$$

Plotting C_D as function of Ri, Fig. 2, shows a peak at $Ri = 1$, or for $U^2 = g\,h\,\cos\theta$. When the current moves with this velocity it is in resonance with long-wavelength waves on the boundary between the current and the ambient water. This resonance draws energy from the current to the waves and it is therefore reasonable that the current experiences higher friction around $Ri = 1$. Notice also that this friction parameter is of the order 10^{-3} for large Richardson number which is of the order used in tidal modelling [Gjevik and Straume, 1989].

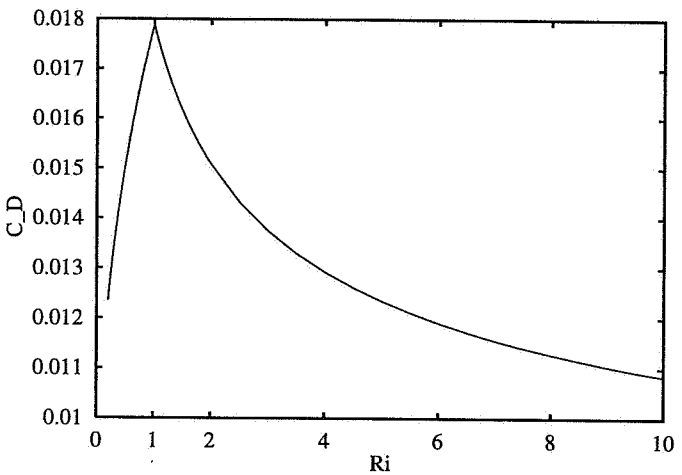

Fig. 2. The Richardson number dependent C_D from Eq. (18).

Price *et al.* [1993], reporting on measurements of the outflow from the Mediterranean through the Gibraltar Strait, give empirical evidence of high friction parameter values. They define bottom stress τ_b (Pa) in the usual manner

$$\tau_b = \rho_0\,C_D\,U^2, \qquad (19)$$

and at the top of the continental slope, which is the site for high acceleration and thereby high entrainment [McCartney, 1992], they found bottom stress of 13 Pa connected to a maximum velocity of 1.3 $\mathrm{m\,s^{-1}}$. With $\rho_0 \sim 10^3$ kg $\mathrm{m^{-3}}$, this gives $C_D = 0.007$. But a mean velocity of the current at say 1 $\mathrm{m\,s^{-1}}$, which is a high estimate, gives $C_D = 0.013$. In our use of the model we have used both the variable and the constant friction parameter approach.

The Appearance of a Singularity in the Model

The inclusion of the pressure term due to variations in the plume thickness, hereafter called the h_ξ-term, gives rise to a singularity. To see this we use the constraint $w/h = constant$ in (5) and (8). Assuming that the variation in density is negligible this results in the following equation for the plume thickness

$$\left(g'\,h - 2\,U^2\right)\,h_\xi = g'h\sin\theta\,\sin\beta - (C_D + 2\frac{\rho_e}{\rho}E)U^2. \qquad (20)$$

The singularity occurs when

$$U^2 = \frac{1}{2}g'h,$$

i.e. when the velocity equals the phase- and group-velocity of internal waves on a current with the constraint that $w/h = constant$ (see Stoker [1957] for analysis of a similar case with current in a channel of constant width).

If during the numerical integration the singularity is approached, the derivative of the current thickness h_ξ will become plus or minus infinity, depending on whether we approach from the subcritical ($U^2 < g'h/2$) or the supercritical ($U^2 > g'h/2$) side, unless the right-hand side is equal to zero simultaneously. In the latter case

$$2\,\sin\theta\,\sin\beta = (C_D + 2\,\frac{\rho_e}{\rho}E), \qquad (21)$$

which gives a critical slope θ. Solutions that pass through this singularity go through a hydraulic jump from subcritical to supercritical flow, or vice versa. This is somewhat similar to the control point analysis for obstacles in a current [Pratt, 1986; Wajsowicz, 1993].

Furthermore, the h_ξ-term includes effects from waves in the momentum equations and thereby the possibility of trig-

gering instabilities. The steady state model cannot treat unsteady waves, indicating that a time dependency should be present when the h_ξ-term is used.

In cases where the singularity has no effect the solutions show no major differences whether the h_ξ-term is present or not. The h_ξ term is therefore neglected in the numerical studies given in this paper. The problem with non-vanishing h_ξ-term will be subject of further studies.

Modelling the Outflow through the Denmark Strait

The Environment and the Numerical Procedure

Dense water formed in the Nordic Seas, i.e., the Greenland, Icelandic and Norwegian Seas, overflow the ridge between Greenland and Iceland (the Denmark Strait), the Iceland-Faroe ridge, and the Faroe-Shetland Channel forming the North Atlantic Bottom Water (NABW) [Dickson *et al.*, 1990].

Our objective is to model the overflow through the Denmark Strait. The surface water contains warm saline water of the Irminger Current and cold but low salinity Polar Water. The intermediate water column is the Arctic Intermediate Water (AIW) with salinity between 34.7 psu and 34.9 psu and with temperature from 0 °C to 1 °C, and Polar Intermediate Water (PIW) with salinity below 34.7 psu and temperatures below 0 °C. At the bottom there is the Norwegian Sea Bottom Water (NSBW) with temperature below 0 °C, typically −0.4 °C, and salinity higher than 34.9 psu, typically 34.94 psu [Malmberg, 1985].

There is some dispute over which water mass contributes to the formation of NABW. Measurements show overflow through the Denmark Strait that experiences an increase in volume transport from a depth of 500m to 2 000m from 2.9 Sv to slightly less than 6 Sv (1 Sv equals 10^6 m^3s^{-1}) [Dickson *et al.*, 1990; Swift *et al.*, 1980]. The initial width over height ratio is 1500. We do not discuss this any further but use these properties of NSBW as initial values for the gravity current.

Using data from Swift *et al.* [1980], we set the ambient potential density σ_{T_θ} to 1027.95 kg m^{-3} and the salinity S to 34.9 psu. The potential density is defined by the expression

$$\sigma_{T_\theta} = \rho(S, T_\theta, P = 0) \qquad (22)$$

where T_θ and P are the potential temperature and the pressure, respectively, and ρ is given by Eq. (11). Our model uses *in-situ* quantities so we have to solve equation (22) with respect to the potential temperature T_θ whereafter we find the absolute temperature from the potential temperature using standard routines [UNESCO, 1983]. When this conversion is done we find the *in-situ* density from the equation of state of seawater.

Equation (22) gives that the potential temperature stays constant but that the *in-situ* temperature increases with depth. This follows from the fact that *in-situ* temperature takes the increasing pressure into account and thereby the compressibility. This also gives rise to the extra driving force, the thermobaric effect, since the current water is colder than the ambient water and therefore is more compressible.

The model is integrated as an initial value problem for S, T, U and β (the initial density is then given from the equation of state) using the *Livermore Solver for Ordinary Differential Equations* [Hindmarsh, 1980]. Relative to the sensitivity for the drag coefficient the solutions are not sensitive to perturbations in the initial values and the numerical study is therefore performed as a sensitivity study for the drag coefficient. The integration is stopped if the plume velocity or the excess density become lower than 10^{-2} m s^{-1} and 10^{-2} kg m^{-3}, respectively.

The Modelled Volume Transport

We estimate the order of magnitude required for the friction parameter in order to obtain an increase in volume transport from 2.9 Sv at 500 m, to slightly less than 6 Sv at 2 000 m [Dickson *et al.*, 1990]. We set the slope angle θ to the value 0.01, and integrate the model for three different constant drag coefficients, $C_D = 0.1$, $C_D = 0.01$ and $C_D = 0.001$, in addition to the Richardson number dependent drag coefficient given by Eq. (18). This gives the volume fluxes shown in Fig. 3. The high drag coefficient solution gives a too small volume flux at 2 000 m, while the two solutions with small C_D have entrained too much ambient water giving too high volume transport. The reason for this is that the current has higher acceleration for the smaller friction cases, so the velocity and the entrainment increase, cf. Eq. (5). The model requires C_D between 0.01 and 0.1 in order to fit measurements. This is less than the requirement of Smith [1975] of $C_D = 0.15$, which was also used by Killworth [1977]. In addition, $C_D = 0.11$ was used by Speer and Tziperman [1990]. The Richardson number dependent friction parameter stays near the $C_D = 0.01$ solution and gives slightly too

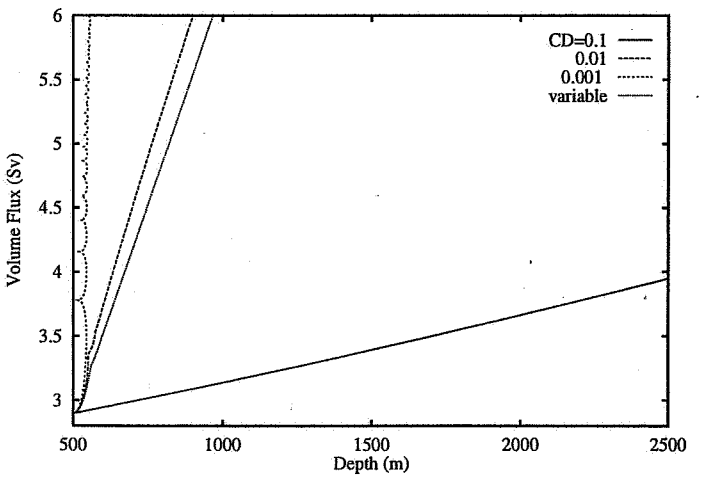

Fig. 3. The modelled volume transport through the Denmark Strait for different friction parameters. Measurements indicates increase in volume transport from 2.9 Sv at 500 m to 6 Sv at 2000 m [Dickson *et al.*, 1990].

much entrainment. Notice also the meander behaviour of the $C_D = 0.001$ solution to be discussed below.

Variable Bottom Topography and a Discussion of Meandering Behaviour

Topographic maps show that the inclination is steeper at 500 meters than at say 1 500 meters. The model can take this into account and we set a steep inclination at 500 m decreasing to zero as indicated in Fig. 4 . This gives the remarkable results shown in Figs. 5 and 6.

When the slope is steep, the gravity term is dominant in the momentum equations, (8) and (9). The low drag solution gains higher velocity than the solution with higher friction parameter. The relative importance of the Coriolis force compared to gravity becomes larger with increasing velocity and with decreasing slope angle θ, which causes the low drag solution to bend fastest of the two cases.

When θ has become smaller the low drag solution oscillates with decreasing amplitude over an equilibrium solution where

$$g(\rho - \rho_e)\sin\theta\cos\beta = \rho f U.$$

This may be explained using conservation of energy arguments. When the plume has high velocity, i.e., high kinetic energy, the Coriolis force bends the current until it moves upwards along the sloping bottom. But as it moves higher, the kinetic energy is lost to potential energy causing the plume to stop the upward motion. When the plume has lost enough kinetic energy for the gravity to overcome the Coriolis force, the current is forced downslope again. This continues until the drag has retarded the current enough to gain force balance. The current then moves in geostrophic balance.

One remark on this oscillatory behaviour has to be made. If the radius of curvature $(\partial\beta/\partial\xi)^{-1}$ become less than half of the plume width, then the model is no longer valid because the plume would cross itself. Nevertheless, it seems that the oscillations do not affect the solutions after the oscillations have come to rest. For instance if the initial velocity is low,

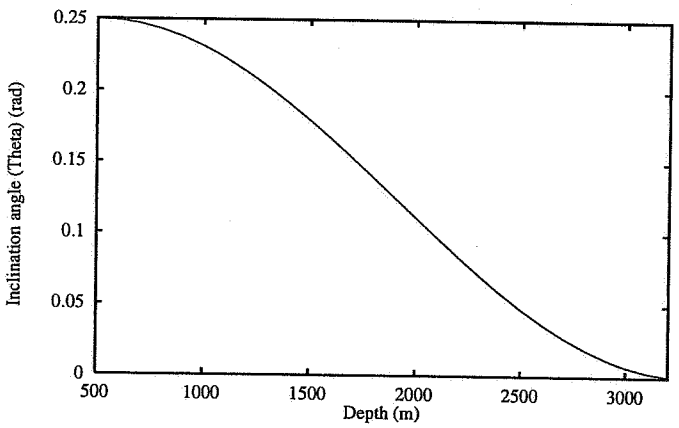

Fig. 4. The inclination angle θ used to study meandering behaviour.

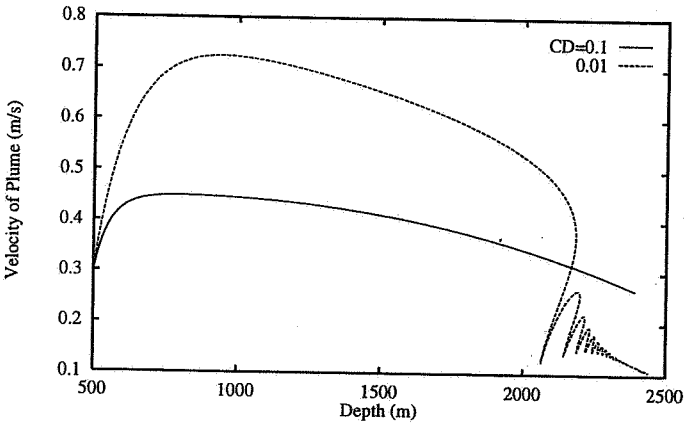

Fig. 5. The plume velocity when the inclined angle varies as shown in Fig. 4. Denmark Strait environment and initial values.

the gravity will accelerate the plume causing similar oscillations as those present in Fig. 5. Another case with higher initial velocity may show similar oscillation but with lower amplitude, but when the oscillations have been damped out the two solutions appear to be equal.

Modelling of Other Deep-Sea gravity Currents

The Weddell Sea Continental Slope

The water in this gravity current, Ice Shelf Water (ISW), is produced from melting under the Ronne Ice Shelf where there exists an upward current with smaller density than the environment [Jenkins, 1991]. This water flows over the Filchner Depression before it flows down the continental slope where it forms the Weddell Sea Bottom Water (WSBW). Killworth [1977] has modelled this gravity current with a model similar to ours, but used gradients instead of *in-situ* quantities for the the ambient water and he also used constant entrainment parameter and drag coefficient.

Using data from Foldvik and Gammelsrød [1988] and Killworth [1977] gives the following quantities: The ambient wa-

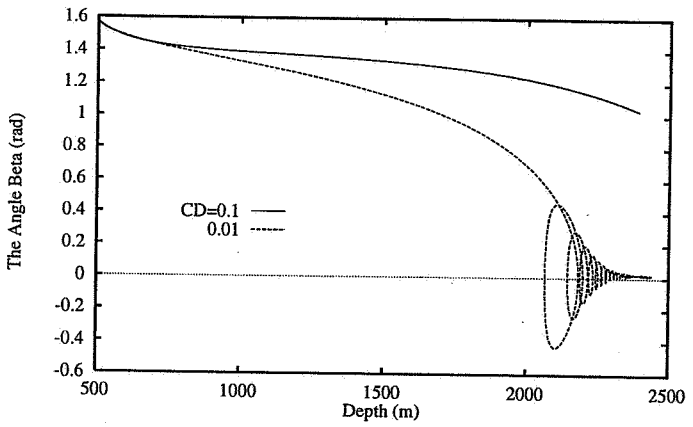

Fig. 6. The angle β as a function of depth when the slope angle decreases as in Fig. 4. Denmark Strait environment and initial values.

ter has potential temperature ranging from 0.0 °C at 500 m to -0.2 °C at 2 000 meters depth. The ambient salinity is between 34.64 psu and 34.72 psu; we use the mean value 34.68 psu. The current is initialized with a volume flux of 0.5 Sv, velocity 0.01 $\mathrm{m\,s^{-1}}$, potential temperature $-1.8\,^{\circ}\mathrm{C}$, and salinity 34.61 psu. The slope is $\theta = 10^{-2}$ rad in the mean directed northward and the plume moves straight downslope at the starting point, i.e. $\beta = \pi/2$ rad. This current is initially very wide and not too high which gives $w\,h^{-1}$ equal to 4 900.

At 2 000 meters depth the volume transport (AU) should increase to 200-300% of the initial value [Killworth, 1977]. The resulting volume transport for different friction parameter is given in Fig. 7. As for the Denmark Strait case, we must have drag coefficient somewhere between $C_D = 0.01$ and $C_D = 0.1$ in order to get the wanted increase in volume transport. In this case however, the variable C_D gives higher entrainment than the $C_D = 0.01$ solution.

Outflow of High Salinity Water from Spencer Gulf, Australia

In the two previous examples of gravity currents the compressibility due to lower temperature inside the current than outside gives rise to an extra driving mechanism. The initial density differences are respectively 0.1 $\mathrm{kg/m^3}$ and 0.01 $\mathrm{kg/m^3}$ for the Denmark Strait and for the Weddell Sea overflows. This effect Killworth [1977] found necessary to include in his plume model in order to let the gravity current down the Weddell Sea continental slope reach as deep as it should according to measurements.

In Spencer Gulf, South Australia, initial excess density in the plume is much higher, 0.6 $\mathrm{kg\,m^{-3}}$, and the compressibility effect has little influence on the current [Bowers and Lennon, 1987; Lennon *et al.*, 1987].

Due to evaporation the Spencer Gulf water becomes saline during summer, and when the high salinity water cools in the autumn it sinks to the bottom and moves out of the gulf

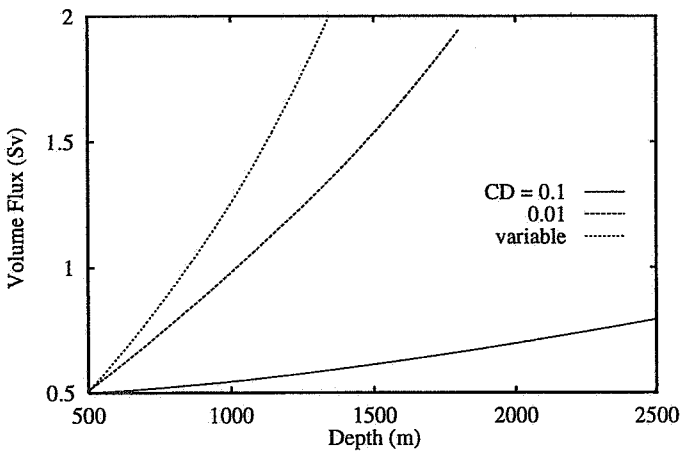

Fig. 7. The modelled volume flux in the Weddell Sea as a function of depth for different drag coefficients. According to Killworth [1977] the volume transport at 2000m should be 1-1.5 Sv.

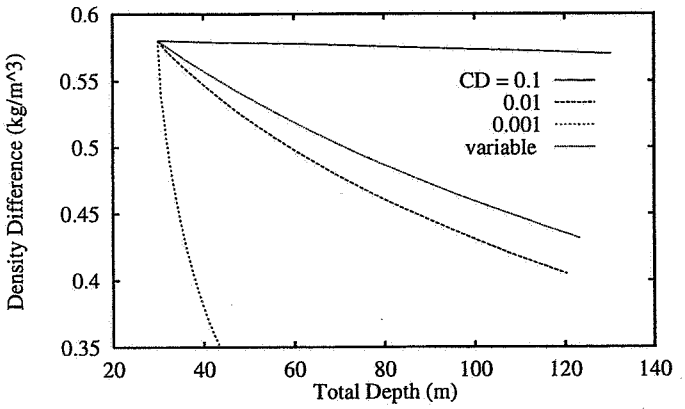

Fig. 8. The density differences for different drag coefficients, in Spencer Gulf.

along the bottom while lighter water moves inwards on top. The volume flux is 0.042 Sv which is much smaller than the corresponding values for the currents treated earlier. The current width over height ratio is set to 1 500.

We have set the ambient temperature to 17 °C and salinity to 36.0 psu. Together with initial values for the current, temperature 16.5 °C and salinity 36.6 psu, this gives the desired density difference of 0.6 $\mathrm{kg\,m^{-3}}$. The slope angle is set to $\theta = 10^{-2}$ rad, and initially the plume moves with angle $\beta \sim \pi/4$ rad [Bowers and Lennon, 1987].

If there was little entrainment, as stated by Bowers and Lennon [1987], then the density differences should stay nearly constant. Fig. 8 shows the modelled density differences for different friction parameters. Notice that the solution with $C_D = 10^{-3}$ gives too much entrainment so in order to fit the measurements we must have higher friction parameter and thereby lower entrainment, as for the previous examples. This is in contrast to the analyzes of Bowers and Lennon [1987] and Lennon *et al.* [1987].

The Gibraltar Strait

Another current mainly driven by high density difference due to high salinity difference is the Mediterranean outflow through the Gibraltar Strait. Again, due to evaporation in the Mediterranean the water gains high salinity and flows out through the Gibraltar Strait with less saline Atlantic water flowing in on top. We start our modelling at 400 meters depth when the current has left the canyon in the strait. The bottom topography is complex in the area, and the current splits into two cores [Ambar and Howe, 1979]. We are therefore not modelling deeper than 900 meter.

The ambient water has salinity 35.8 psu and potential density 1027 $\mathrm{kg\,m^{-3}}$, giving a temperature of 13.1 °C. The initial volume flux of the currents is set to 2 Sv with salinity 38.0 psu and temperature 13.2 °C[Price *et al.*, 1993; Ochoa and Bray, 1991]. This gives density difference $\sim$ 1.68 $\mathrm{kg\,m^{-3}}$ which is somewhat higher than used by Smith [1975] (1.25 $\mathrm{kg\,m^{-3}}$). The inclination is set to 0.015 rad and the width to thickness ratio is estimated to 47 [Smith, 1975]. At 700 - 900

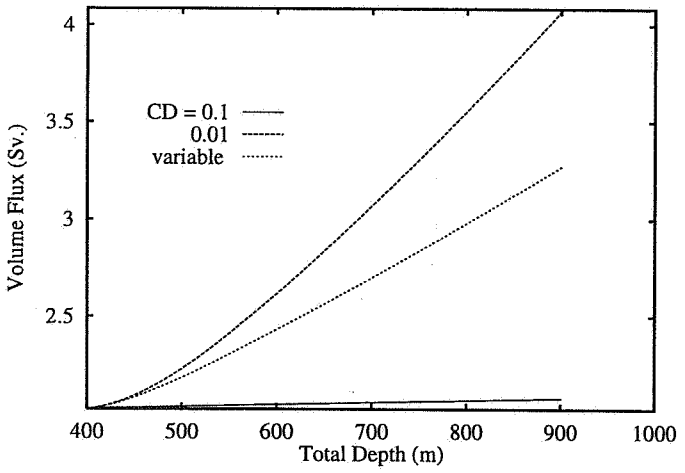

Fig. 9. The modelled volume flux for different drag coefficients in the Gibraltar Strait. Measurements indicates 2 Sv at 400m with an increase of approx. 0.6 Sv at 900 m [Price *et al.*, 1993].

m depth the observed volume flux increases by 0.6 Sv and the density anomaly decreases to 0.7 kg m^{-3} [Price *et al.*, 1993].

The variable friction parameter in this case turns out like 0.015. Results from our modelling shows that this friction parameter fits the observed volume flux (Fig. 9) best, while the low constant friction parameter 0.01 fits the observed density difference best (Fig. 10). Thus our model does not identify a unique friction parameter for this case. This indicates that there may be missing physics in the model. One possibility may be variable bottom friction. The way we defined the dependency in Eq. (18) it represents friction on the interface between the current and the ambient water. Price *et al.* [1993] shows with support in measurements that the bottom friction can be higher than the interfacial friction.

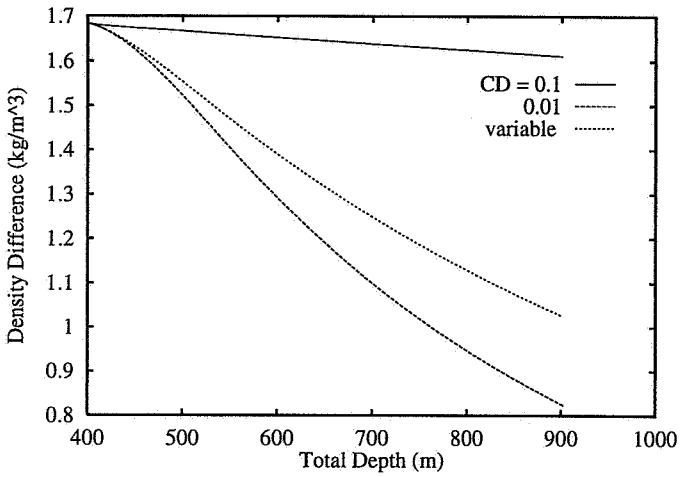

Fig. 10. The modelled density differences for different drag coefficients in the Gibraltar Strait. According to measurements the density anomal should decrease from $\sim$ 1.7 kg m^{-3} at 400 m to 0.7 kg m^{-3} at 700 -900 m [Price *et al.*, 1993; Ochoa and Bray, 1991].

Fig. 11 shows the resulting friction parameter from Eq. (18) for three of the cases reported in this paper. In the shallower Spencer Gulf case case the friction parameter starts at 8×10^{-3} decreasing to approximately 5×10^{-3}.

Conclusions

An extensive description of an integrated plume model is given and derivation of the pressure term due to variations in plume thickness is included. This term includes waves in the momentum equations and thereby the possibility of net energy loss to wave energy and instabilities. At low friction, meandering behaviour is to be expected. This may occur e.g. in the downstream part of the overflow from the Denmark Strait. Further study of waves and meanders would require a time dependent model.

We used an entrainment parameterization based on empirical data, and introduced a drag coefficient consistent with the entrainment parameter. Within the limitation of the steady state model, the numerical results shows that the friction parameter should be between 0.01 and 0.1 in order to provide an order of magnitude fit to measurements. The consistent Richardson dependent drag coefficient gives solutions that give too little entrainment but this drag coefficient parameterizes only the interfacial friction so additional bottom friction should perhaps be added. This study indicates that gravity current modelling should use friction values approximately a factor ten higher than used for instance in tidal modelling. This may be important for the representation of such currents in large scale climate models.

Appendix: Derivation of The Integrated Plume Model

The configuration is as given in Fig. 1.

The Local Governing Equations

An infitesimal volume inside the current follows the local

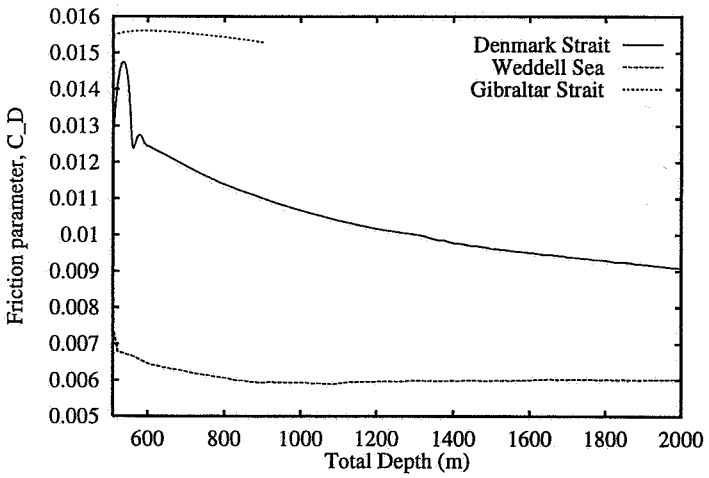

Fig. 11. The resulting drag coefficient, C_D, for three of the currents. In Spencer Gulf, not shown, the frictrion parameter starts at approx. 0.008 decreasing to approx. 0.005

continuity equation and the equation of motion which reads for steady state:

$$\nabla \cdot \rho_l \, \mathbf{u} = 0, \tag{23}$$

$$\rho_l \mathbf{u} \cdot \nabla \mathbf{u} = \mathcal{F} + \nabla \cdot \tilde{\tau}, \tag{24}$$

where ρ_l ($\mathrm{kg\,m^{-3}}$) is the local density, $\mathbf{u}$ ($\mathrm{m\,s^{-1}}$) the local velocity, $\mathcal{F}$ is the volume force, and $\tilde{\tau} = \tau_{ij}\mathbf{e}_i\mathbf{e}_j$ ($\mathbf{e}_i$ and $\mathbf{e}_j$ being unit vectors), the stress tensor, represents forces acting on the boundary of the volume. Volume forces in our study are gravity ($\mathcal{F}_{grav} = -g\rho_l\mathbf{k}$), and Coriolis force ($\mathcal{F}_{coriolis} = -2\rho_l\boldsymbol{\Omega} \times \mathbf{u}$), where $\boldsymbol{\Omega}$ ($\mathrm{s^{-1}}$) is the angular velocity of the earth.

The first subscript of the stress tensor indicate the direction in which the normal to the plane is pointing while the second subscript indicates the direction in which the force is acting. This means that the diagonal elements (τ_{ii}) represent forces which are acting normal to the surface while those elements with different subscripts (τ_{ij}, $i \neq j$) are shear forces.

Let $-p = \tau_{11} + \tau_{22} + \tau_{33} = trace(\tilde{\tau})$, then the local steady state momentum equation may be written:

$$\rho_l \mathbf{u} \cdot \nabla \mathbf{u} = \mathcal{F} - \nabla p + \nabla \cdot (\tilde{\tau} - trace(\tau)\tilde{\mathcal{I}}) \tag{25}$$

where $\tilde{\mathcal{I}}$ is the unit dyad.

The pressure is assumed to be hydrostatic. Fig. 12 illustrates a section through the current in the along stream direction. A reference particle moving a distance $\Delta\xi$ in the along-stream direction experiences an increase in pressure given by the expression

$$p(\xi + \Delta\xi) = p(\xi) + g\rho_e \, (\Delta\xi \sin\phi - r) + g\rho r, \tag{26}$$

where ρ is the mean density of the current to be defined.

Simple geometric relations and Taylor expansion to second order in $(\Delta\xi - s)$ gives:

$$\begin{aligned} r\sin\phi &= s, \\ r\cos\phi &= h\,(\xi + \Delta\xi - s) - h\,(\xi) \\ &= \tfrac{dh}{d\xi}\,(\Delta\xi - s) + O\left((\Delta\xi - s)^2\right). \end{aligned} \tag{27}$$

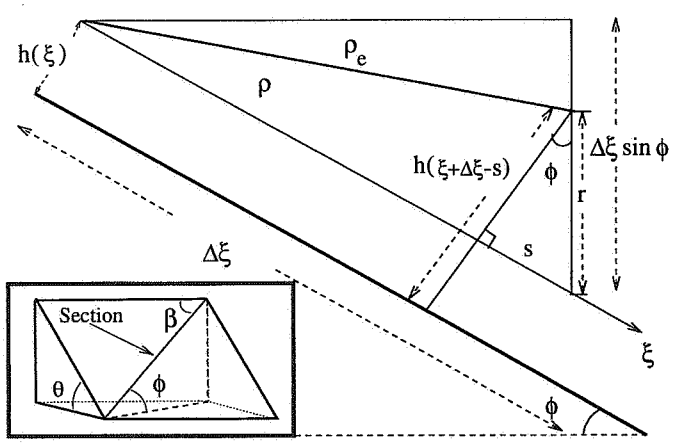

Fig. 12. Illustration of the pressure term.

For small ϕ we have that

$$r = \Delta\xi \, \frac{\partial}{\partial\xi} h. \tag{28}$$

Using (28) in (26) and letting $\Delta\xi \to 0$ gives that

$$\frac{\partial}{\partial\xi} p = g\,\rho_e \, \sin\theta \sin\beta + g\,(\rho - \rho_e)\,\frac{\partial}{\partial\xi} h, \tag{29}$$

where the identity $\sin\phi = \sin\theta\sin\beta$ has been used (see inset in Fig. 12).

In the other directions the variation in plume thickness has no effect, so

$$\frac{\partial}{\partial\eta} p = g\,\rho_e \, \sin\theta\,\cos\beta, \quad \frac{\partial}{\partial z'} p = g\,\rho_e\,\cos\theta. \tag{30}$$

Integration of the Local Equations

The plume model represents the overall behaviour of the current, so the mean values of velocity, density, salinity, etc., are studied while interior structures from turbulence are neglected. The model equations are obtained by integration of the local governing equations over a cross-section of the current normal to the along-stream direction. The cross-section has area A, width w and thickness h; $A = w \cdot h$. The mean over the cross section is defined as

$$B = \frac{1}{A} \int_0^h \int_{-w/2}^{w/2} b \, d\eta \, dz', \tag{31}$$

where b is an arbitrary local scalar or vector quantity.

Conservation of mass. The continuity equation integrates and gives

$$\frac{\partial}{\partial\xi}(A\,\rho\,U) = \rho_e w v_e = \rho_e w E U, \tag{32}$$

where ρ is the mean density of the current and where the entraining velocity v_e ($\mathrm{m\,s^{-1}}$) is set proportional to the mean velocity U of the current, [Smith, 1975]. For a wall bounded currents the entrainment parameter E is strongly related to the overall Richardson number, Eq. (13) [Turner, 1973].

Conservation of salt and heat. In the same manner as for the total mass conservation, continuity equations have to be valid for the salinity and for the internal energy (heat). The salinity S is defined as gram salt per kilogram water so, similar to the conservation of total mass, the conservation equation of salt reads

$$\frac{\partial}{\partial\xi}\,(S\,\rho\,A\,U) = \rho_e S_e E(Ri_0) w U. \tag{33}$$

Neglecting energy sources such as heat production due to friction gives in a same manner the internal energy conservation equation

$$\frac{\partial}{\partial\xi}\,(\rho\,C_p\,T_K\,A\,U) = \rho_e C_p T_{K,e} E(Ri_0) w\,U. \tag{34}$$

Here T_K (K) is the absolute temperature and C_p ($\mathrm{J\,m^{-3}\,K^{-1}}$) the heat capacity of the fluids. Since C_p for

the ambient water approximates the heat capacity for the current water and remains almost constant with ξ, we have that

$$\frac{\partial}{\partial \xi}(\rho T_K A U) = \rho_e T_{K,e} E(Ri_0) w U. \quad (35)$$

The equations of motion. Neglecting turbulent fluctuations perpendicular to the along stream direction (assuming that they sum up to zero) means that the left hand side of (24) becomes

$$\rho_l u \frac{\partial}{\partial \xi} u \mathbf{e}_\xi + \rho_l u^2 (\frac{\partial}{\partial \xi}\beta)\mathbf{e}_\eta. \quad (36)$$

The local continuity equation gives that $\partial(\rho_l u)/\partial\xi = 0$, and assuming that $u \to 0$ at the boundary between the current and the ambient water, integration of (36) over the cross-section gives

$$\frac{\partial}{\partial \xi}\left(A\rho U^2\right)\mathbf{e}_\xi + A\rho U^2\left(\frac{\partial}{\partial \xi}\beta\right)\mathbf{e}_\eta. \quad (37)$$

Here we have assumed that the mean of ρU is equal to the mean density times the mean velocity.

Integrating the divergence of the stress tensor gives

$$\int\int_A \nabla\cdot\left(\tilde{\tau} - trace(\tau)\tilde{\mathcal{I}}\right) dA \equiv \int\int_A \nabla\cdot\tilde{\mathcal{D}}\, dA = \int_\Gamma \tilde{\mathcal{D}}\, d\Gamma, \quad (38)$$

where Γ is the boundary of the cross-section. We distinguish between stresses normal and tangential to the boundary. The normal stresses are due to a force from the bottom responding on the weight of the plume and the hydrostatic pressure acting on the top of the plume, we call this N and it points in the z' direction.

The shear stress must oppose the movement of the current. We assume the usual drag law, proportional to the square of the velocity and to the width of the current, so

$$\int_\Gamma \tilde{\mathcal{D}}\, d\Gamma = N\mathbf{k}' - C_D w U^2 \mathbf{e}_\xi. \quad (39)$$

Integration of the gravity and Coriolis terms follows trivially so the equations of motion read:

$$\frac{d}{d\xi}\left(\rho A U^2\right) = Ag(\rho - \rho_e)(\sin\theta\sin\beta - \frac{dh}{d\xi}) - C_D w U^2, \quad (40)$$

$$\rho U^2 \frac{d}{d\xi}\beta = g(\rho - \rho_e)\sin\theta\cos\beta - \rho f U, \quad (41)$$

$$0 = -g(\rho - \rho_e)\cos\theta - \rho f_k U + N. \quad (42)$$

Here $f = 2\,\Omega\,(\sin\varphi\cos\theta - \cos\varphi\sin\theta\sin\zeta)$ is the Coriolis parameter, φ being the latitude and ζ being the orientation of the slope; for $\zeta = 0$ the slope sinks in the eastward direction, while $\zeta = \pi/2$ means that the slope is in the north direction [Alendal *et al.*, 1993]. The Coriolis parameter f_k has a lengthier expression but since the normal force N acting from the bottom on the current opposes the weight of the plume, it responds in such a manner that equation (42) is always satisfied and this equation is not of interest.

Acknowledgments. This work originated from a project supported by Den Norske Stats Olje Selskap (Statoil), Norsk Hydro a.s., the Norwegian State Pollution Authority (SFT) and the Norwegian Research Council. GA is presently supported by the Norwegian Research Council and HD is supported by Saga Petroleum a.s.

References

Alendal, G., H. Drange, and P. M. Haugan, Injection of CO_2 in the ocean: Modelling bottom gravity currents with CO_2-enriched seawater, Technical Report 66A, Nansen Environmental and Remote Sensing Center, 1993.

Ambar, I. and M. R. Howe, Observation of the Mediterranean outflow - I: Mixing in the Mediterranean outflow, *Deep-Sea Res.*, **26A**:535–554, 1979.

Bowers, D. G. and G. W. Lennon, Observations of stratified flow over a bottom gradient in a coastal sea, *Cont. Shelf Res.*, **7**(9):1105–1121, 1987.

Christodoulou, G. C., Interfacial mixing in stratified flows, *J. Hydr. Res.*, **24**(2):77–92, 1986.

Dickson, R. R., E. M. Gmitrowicz, and A. J. Watson, Deep-water renewal in the northern North Atlantic, *Nature*, **344**:848–850 1990.

Drange, H., G. Alendal, and P. M. Haugan, P. M. A bottom gravity current model for carbon-dioxide enriched sinking seawater, *Energy Conv. Mgmt.*, **34**(9-11):1065–1072, 1993.

Foldvik, A. and T. Gammelsrød, Notes on southern hydrography, sea-ice and bottom water formation, *Palaeogeogr. Palaeoclimatol. Palaeoecol.*, **67**:3–17, 1988.

Gjevik, B. and T. Straume, Model simulations of the m_2 and the k_1 tide in the Nordic seas and the Artic ocean, *Tellus*, **41 A**:73–76, 1989.

Haugan, P. M. and H. Drange, Sequestration of CO_2 in the deep ocean by shallow injection, *Nature*, **357**:318–320, 1992.

Hindmarsh, A. C., LSODE and LSODI, two new initial value ordinary differential equation solvers, *ACM-Sign. Newsl.*, **15**:10–11, 1980.

Jenkins, A., A one-dimensional model of ice shelf-ocean interaction, *J. Geophys. Res.*, **96**(C11):20,671–20,677, 1991.

Killworth, P. D., Mixing on the Weddell sea continental slope, *Deep-Sea Res.*, **24**:427–448, 1977.

Killworth, P. D., Deep convection in the world ocean, *Rew. Geophys. Space Phys.*, **21**(1):1–26, 1983.

Lennon, G. W. *et al.*, Gravity currents and the release of salt from an inverse estuary., *Nature*, **327**:695–697, 1987.

Malmberg, S.-A., The water masses between Iceland and Greenland, in *Chemical tracers for studying water masses and physical processes in the sea*, edited by Stefánsson, U., volume IX, RIT Fiskideildar, 1985.

McCartney, M. S., Recirculating components to the deep boundary current of the northern North Atlantic, *Prog. Oceanog.*, **29**:283–383, 1992.

Morton, B. R., G. I. Taylor, and J. S. Turner, Turbulent gravitational convection from maintained and instantaneous sources, *Proc. Roy. Soc. A*, **234**:1–23, 1956.

Oberhuber, J. M. Simulation of the Atlantic Circulation with a coupled Sea Ice -Mixed Layer - Isopycnal General Circulation Model, Part I: Model Description, *J. Phys. Oceanogr.*, **23**(5):808–829, 1993.

Ochoa, J. and N. A. Bray, Water mass exchange in the Gulf of Cadiz, *Deep-Sea Res.*, **38**(Suppl 1):S465–S503, 1991.

Pratt, L. J., Hydraulic control of sill flow with bottom friction, *J. Phys. Ocanogr.*, **16**:1970–1980, 1986.

Price, J. F., M. O'Neill Baringer, R. G. Lueck, G. C. Johnson, I. Ambar, G. Parilla, A. Cantos, M. A. Kennelly, and T. B. Sanford, Mediterranean outflow mixing and dynamics, *Science*, **259**:1277–1282, 1993.

Rudnicki, M. D. and H. Elderfield, Theory applied to the Mid-Atlantic Ridge hydrothermal plumes; the finite-difference approach, *J. Volc. and Geoth. Res.*, **50**:161–172, 1992.

Simpson, J. E., *Gravity currents in the environment and the laboratory*, Halsted Press, Chichester, 1987.

Smith, P. C., A streamtube model for bottom boundary currents in the ocean, *Deep-Sea Res.*, **22**:853–873, 1975.

Speer, K. and E. Tziperman, Convection from a source in an ocean basin, *Deep-Sea Res.*, **37**(3):431–446, 1990.

Stigebrandt, A. A model for the vertical circulation of the Baltic deep water, *J. Phys. Oceanogr.*, **17**:1772–1785, 1987.

Stoker, J. J., *Water Waves*, Interscience Publishers Inc, New York, 1957.

Swift, J. H., K. Aagaard, and S.-A. Malmberg, The contribution of the Denmark Strait overflow to the deep north atlantic, *Deep-Sea Res.*, **27A**:29–42, 1980.

Turner, J. S., *Buoyancy effects in fluids*, Cambridge University Press, Cambridge, 1973.

UNESCO, Tenth report of the joint panel on oceanographic tables and standards, UNESCO Tecnical Papers in Marine Sci. 36, Paris, 1981.

UNESCO, Algoritm for computation of fundamental properties of seawater, UNESCO tecnical papers in marine science 44, Paris, 1983.

Wajsowicz, R. C., Dissipative effects in inertial flows over a sill, *Dyn. Atmosph. Oceans*, **17**:257–301, 1993.

Woods, A. W., The fluid dynamics and thermodynamics of eruption columns, *Bull. Volcanol.*, **50**:169–193, 1988.

Guttorm Alendal, Helge Drange and Peter M. Haugan, Nansen Environmental and Remote Sensing Center, Edvard Griegsvei 3a, N–5037 Solheimsviken/Bergen, Norway.